DYNAMIC PROGRESSIVE COLLAPSE OF HIGH-RISE BUILDINGS

SAID A. ELKHOLY AND KIMIRO MEGURO
Institute of Industrial Science, University of Tokyo
4-6-1 Komaba, Meguro-ku, Tokyo 153-8505, Japan

ABSTRACT

The progressive failure occurs due to changing in loading pattern, boundary condition, or loading capacity in some structural elements which may result in the failure of another structural element(s). The collapse of Ronan Point apartment building in England in 1968 had been introduced evidently this phenomena. More destructive events had been shown recently like: the progressive collapse of Alfred P Murrah building in Oklahoma City, 1995 and the WTC towers in New York, 2001. Studying those evidences and others requires a powerful numerical tool to analyze the structure failure stages. Among the available numerical tools the Applied Element Method (AEM) is known as a numerical model capable of analyzing the complete structure behavior from early stage of loading till complete collapse with reliable accuracy. However, in order to guarantee stability and accuracy of solution, the number of may be large indeed which increases the computer power and time needed for numerical simulation. The numerical tools must be able to capture pre-failure behavior accurately in order to capture the behavior of the real structure during failure. So, it is necessary to search for a new technique requiring less computer time and effort to model a structure.

This paper describes the methodology of Improved Applied element method, an advanced analysis technique for studying the total behavior of steel structures subject to different hazard loads. The CPU time for the improved applied element method is very small compared with conventional AEM). Using improved AEM method can help engineers to investigate the performance of the steel tall buildings under different hazardous loads. The mechanism of progressive failure and the effect on the neighboring buildings as well can be also simulated. Numerical examples showing the accuracy, efficiency, and the range of application of the improved method are presented.

1. INTRODUCTION

Only a brief introduction to the two-dimensional Applied Element Method is given here. The AEM is a recently developed technique for structural analysis (Meguro and Tagel-Din, 1997). The application of AEM to structural analysis is recognized as a powerful tool for analyzing the structural behavior from early stage of loading and up to the total collapse occurs (Tagel-Din and Meguro, 2000[a] and Tagel-Din and Meguro, 2000[b]).

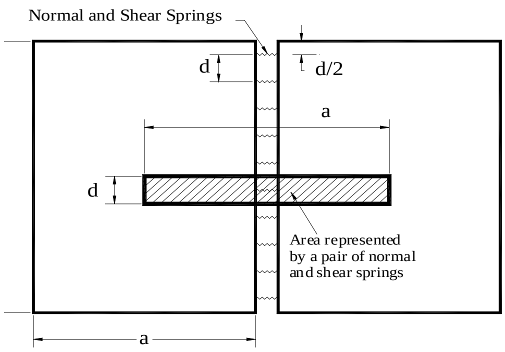

Figure 1: Area of influence of each pair of springs

In AEM, the structure is modeled as an assembly of small rigid square elements. In two dimensions, each element has three degrees of freedom. A pair of elements is connected with pairs of normal and shear springs uniformly distributed on the boundary line. Each pair of springs totally represents stresses and deformations of a certain area (hatched area in Figure 1) of the studied elements. Therefore, the normal and shear stiffness can be determined by Equation 1.

$$K_n = \frac{E * d * T}{a} \quad \text{and} \quad K_s = \frac{G * d * T}{a} \tag{1}$$

where d is distance between each spring; a is length of representative area; *E* and *G* are Young's and shear modules of the material, respectively; and *T* is the thickness of element, which is considered constant for all springs attached to the element (Meguro and Tagel-Din, 2000 and Meguro and Tagel-Din, 2001).

The springs represent the microscopic material properties, such as stiffness and yield strength. The conventional AEM used in different engineering field has shown high accuracy and applicability for modeling reinforced concrete, soil and masonry. However, some applications are difficult to handle like huge steel structure buildings. Using the current version of AEM, elements with very small size should be used to follow the change in the thickness especially in non-rectangle cross sections (i.e. I Shape, Channel, and Boxed sections), since the element should be chosen to fit the flange thickness. In this paper, we introduce the Improved Applied Element Method which can easily handle this type of cases.

2. IMPROVED APPLIED ELEMENT METHOD (IAEM)

Two major extensions of the AEM have been implemented: improving the element type to be able to follow any change in the non-rectangle cross-section thickness, and allowing different thickness to be used for calculating normal stiffness and shear stiffness. That kind of modification allows using large elements, having the same cross sectional geometric parameters like normal, shear and bending stiffness. The value of normal and shear stiffness for each springs pair can be determined by Equation 2.

$$K_n^i = \frac{E \cdot d \cdot T_n^i}{a} \quad \text{and} \quad K_s^i = \frac{G \cdot d \cdot T_s^i}{a} \tag{2}$$

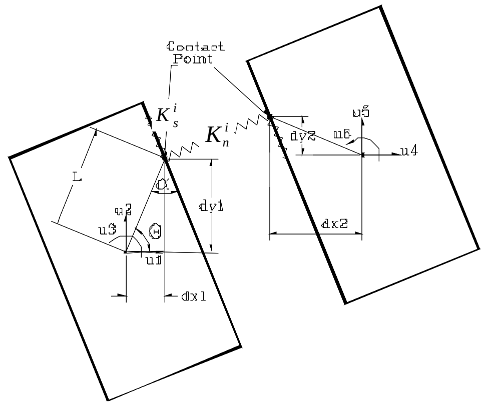

Figure 2: Contact Point and D.O.F

where: T_n^i and T_s^i are the thickness represented by the springs pair "*i*" for normal and shear cases, respectively. That difference in the value of T_n^i and T_s^i owes to the change in effective area for both of normal and shear directions

A pair of rigid elements, as shown in Figure 2, are assumed to be connected by only one pair of normal sprig stiffness (K_n^i) and shear spring stiffness (K_s^i). The values of dx and dy correspond to the relative coordinate of the contact point with respect to the center of gravity. To have a global stiffness matrix, the location of elements and contact springs are assumed in a general position. The stiffness matrix components corresponding to each degree of freedom are determined by assuming a unit displacement in the studied direction and by determining forces at the centroid of each element. The element stiffness matrix size is only (6 x 6). Equation 3 shows the components of the upper left quarter of the stiffness matrix. All used notations in this equation are shown in Figure 2. It is clear that the stiffness matrix depends on the contact spring stiffness and the spring location.

$$\left[\begin{array}{c|c|c} \begin{array}{l} Sin^2(\theta+\alpha)K_n^i \\ +Cos^2(\theta+\alpha)K_S^i \end{array} & \begin{array}{l} -K_n^i Sin(\theta+\alpha)Cos(\theta+\alpha) \\ +K_S^i Sin(\theta+\alpha)Cos(\theta+\alpha) \end{array} & \begin{array}{l} Cos(\theta+\alpha)K_S^i LSin(\alpha) \\ -Sin(\theta+\alpha)K_n^i LCos(\alpha) \end{array} \\ \hline \begin{array}{l} -K_n^i Sin(\theta+\alpha)Cos(\theta+\alpha) \\ +K_S^i Sin(\theta+\alpha)Cos(\theta+\alpha) \end{array} & \begin{array}{l} Sin^2(\theta+\alpha)K_S^i \\ +Cos^2(\theta+\alpha)K_n^i \end{array} & \begin{array}{l} Cos(\theta+\alpha)K_n^i LCos(\alpha) \\ +Sin(\theta+\alpha)K_S^i LSin(\alpha) \end{array} \\ \hline \begin{array}{l} Cos(\theta+\alpha)K_S^i LSin(\alpha) \\ -Sin(\theta+\alpha)K_n^i LCos(\alpha) \end{array} & \begin{array}{l} Cos(\theta+\alpha)K_n^i LCos(\alpha) \\ +Sin(\theta+\alpha)K_S^i LSin(\alpha) \end{array} & \begin{array}{l} L^2Cos^2(\alpha)K_n \\ +L^2Sin^2(\alpha)K_S^i \end{array} \end{array}\right] \tag{3}$$

Although in this method, we can change the characteristics of all springs surrounding any element, in practical use, only changing in the corner springs is needed for steel flanged sections. As shown in Figure 3, changing in the ratios of (K_1/K_2) and (K_3/K_4) can control the stiffness of any element. That kind of improvement allows using many different flanged steel sections like I-beam, Box and Channel cross sections. Moreover, any cross section can be simulated by adjusting the values of element height, number of springs, ratio between outer to inner thickness, and ratio between normal to shear thickness.

The change in each spring thickness is also considered for accounting the dynamic characteristics of each element. The mass matrix and the polar

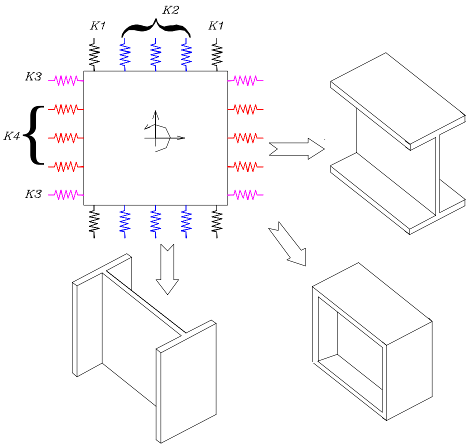

Figure 3: Element Shape for Improved AEM

moment of inertia of each element have been idealized as lumped at the element center of gravity. The values of those lumped mass in each DOF direction can be calculated by summing the effect of the small segmental mass represented by each spring considering the change of springs' thickness, as shown in Equation 4.

$$\begin{bmatrix} M1 \\ M2 \\ M3 \end{bmatrix} = \begin{bmatrix} D^2 * t_{av} * \rho \\ D^2 * t_{av} * \rho \\ \frac{D^4 \cdot \rho}{nsp} \cdot \sum_{i=1}^{i=nsp} \left(\frac{t_i^x}{12} + \frac{t_i^y}{12}\right) \end{bmatrix} \tag{4}$$

where: D is the element size; t_{av} is the average thickness of the element; ρ is the density of material considered; *nsp* is the number of connecting springs; and t_i^x and t_i^y are the i^{th} spring thickness in x and y direction respectively.

3. NUMERICAL EXAMPLES AND RESULTS

In order to evaluate the accuracy of the proposed IAEM and to illustrate the applicability of the method, two verification examples are presented in this section.

Example 1: Long span steel beam

The first example is the 2-D steel beam of 11.25 m span. The dimensions, supports, loading conditions, and cross section are shown in Figure 4. The deflection at the mid span of the beam was calculated by using both previous AEM and IAEM versions. The Young's Modulus is 200 GPa and

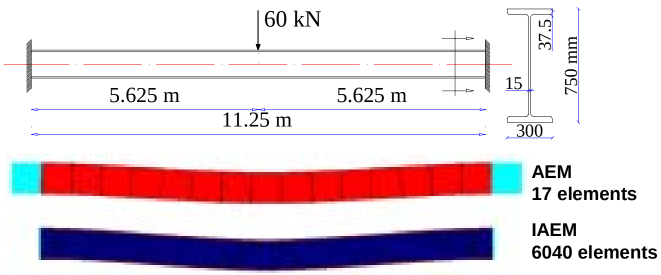

Figure 4: Fixed Beam Loaded in Mid-span

elastic analysis was performed using both of two models. Element size is taken as total height of the cross section in IAEM case. The ratio between outer and inner springs' stiffness was taken as 20 (the same ratio between flange width and web thickness). With the IAEM, 17 general shaped elements are used including two boundary elements. However, 6040 square elements with a constant thickness, including 40 elements for boundary condition, are utilized to model the same beam using original AEM code. The results are compared to the theoretical results considering both bending and shear deformations as listed in Table 1. From the table, it can be concluded that by using less number of elements, CPU time required is drastically reduced and the accuracy was better with the IAEM compared with AEM.

Table 1: Comparison between AEM and IAEM Model results

	No. of elements	**Element size (cm^2)**	**No. of DOF**	**CPU Time**	**Deflection (mm.)**	**Error Comparing with theoretical value (%)**
AEM	6040	3.75*3.75	18000	120 sec	0.900	+2.31%
IAEM	17	75*75	45	Less than one sec.	0.866	-1.59 %

Example 2: Dynamic analysis of fifteen-story two-bay frame structure

In order to evaluate the accuracy of IAEM in dynamic analysis, a 15 story- two bay two-dimensional frame structure, as shown in Figure 5, is considered in this study. All the beams and column are assumed to have the same I-beam section represented in Figure 5. The Young's modulus of 200 GPa is used. The analysis is performed using 870 elements with IAEM; however 543,750 elements should be used to simulate the same structure by using previous version of AEM. The natural frequencies of the structure are calculated and listed in Table 2. The first 8 modes, obtained from IAEM and SAP 2000 (CSI, 2000), are close and a maximum difference of 1.63 % has been observed. Those eight mode shapes are shown in Figure 6.

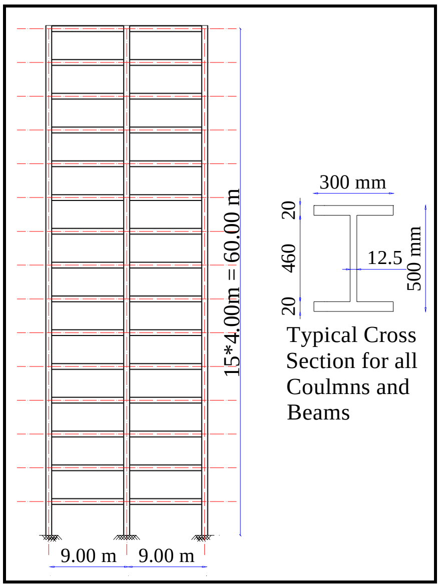

Figure 5: 15-story Two-bay Frame

Table 2: The Results of Model Analysis (Frequency, Hz)

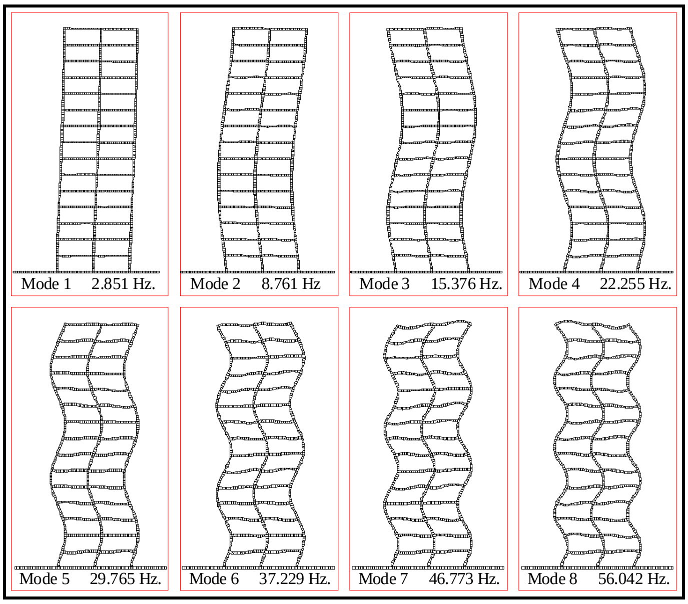

Figure 6: First Eight Calculated Modes using IAEM

The verification examples demonstrate the accuracy and efficiency of the IAEM. Moreover, less computational effort and a wider applicability for structural analysis have been noted. The good agreement with both theoretical and finite element results in linear static and dynamic load condition illustrates the applicability of the proposed method in parametric studies of components and structures subject to different hazardous loading.

4. FAILURE ANALYSIS OF HIGH-RISE STEEL BUILDING

A four-bay 30-story steel frame building is investigated in this study. The structural configuration of the building is shown in Figure 7. The typical story height is 4.00 m. 2520 elements were utilized for modeling the whole structure using IAEM. The frame has been exposed to extreme fire loading condition at the 22nd floor level. The fire has been assumed to produce reduction in steel stiffness and strength of a part of beams and attached columns at that level. Figure 8 shows the numerical simulation results of the collapse mechanism of the frame structure. From the numerical analysis, the progressive failure of the structural frame had initiated by softening of steel beam, which produced large displacements. Following the structural elements started to fail, buckling occurred to the steel columns due to the change of end conditions, as shown in Figure 8(b). When the columns or floor connections failed,

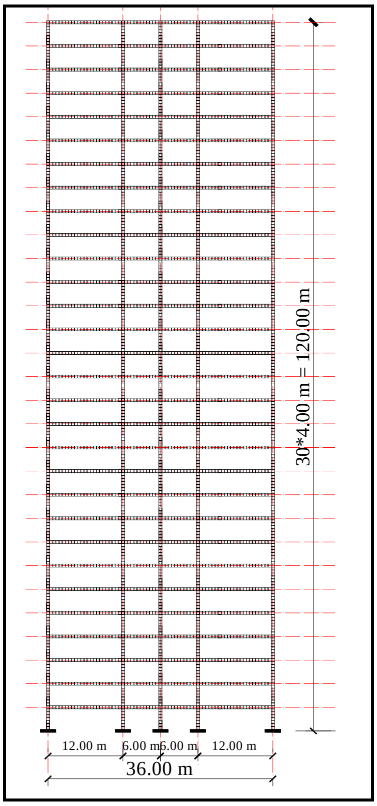

Figure 7: Frame model

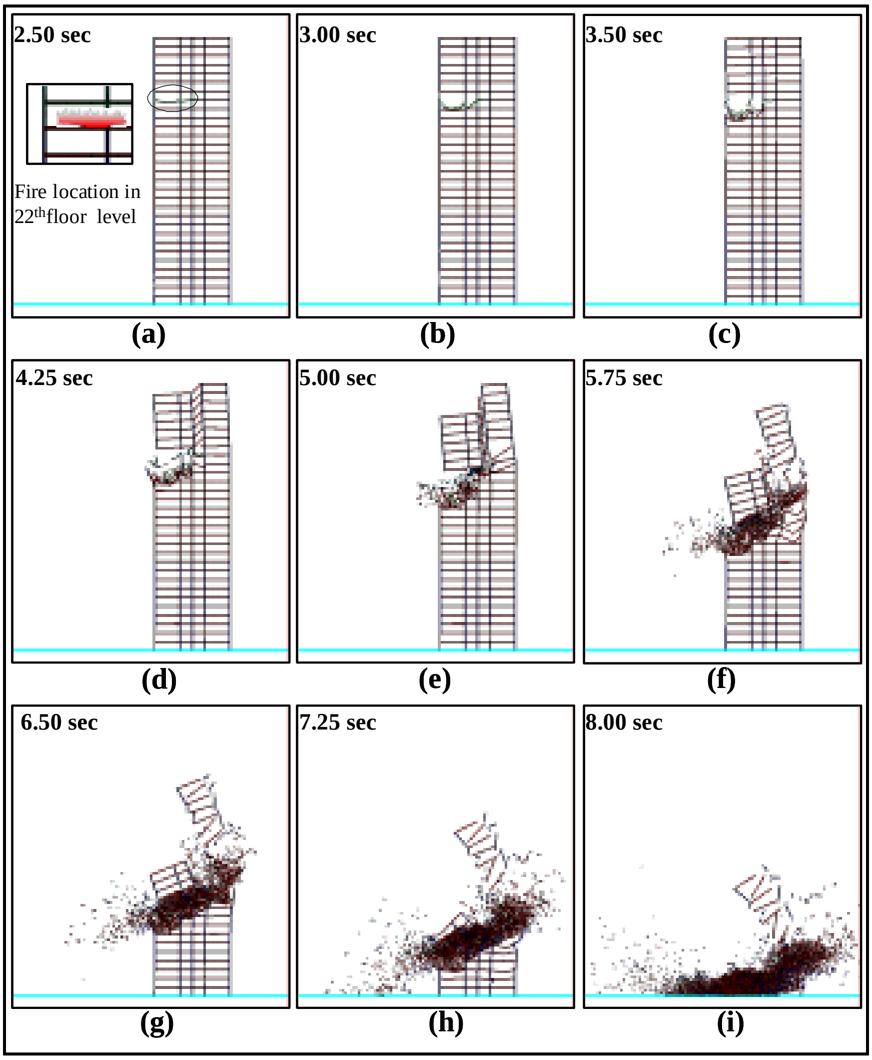

Figure 8: Failure Mechanism of 30-story Steel Structure

the structural loading was no longer static, but dynamic. Once one floor fell onto another, a domino effect could be observed. The impact of one floor falling on the floor below creates a huge amount of force. As each floor fell, this force would increase until the bottom.

The numerical simulation shows the mechanism of failure of a high-rise steel structure under the effect of severe fire condition. The analysis explains how partial damage in certain structural element can produce total collapse of the building. The numerical simulation is qualitatively similar to the recorded sequence of collapse of North Tower in World Trade Center, shown in Figure 9.

5. CONCLUSIONS

The numerical simulation method, IAEM, presented in this paper shows a good capability to study the total behavior of structural buildings from early stage of loading until the total collapse occurs. The validity of the developed code has been demonstrated by several numerical examples. The verification examples indicate that IAEM shows a good agreement with both theoretical and finite element results in linear static and dynamic load condition. Moreover, less computational effort and a wider applicability for

Figure 9: Sequence of collapse of North Tower of WTC (Photo from CNN)

structural analysis have been observed than conventional discrete element methods. The collapse process of high-rise steel structure model under extreme localized fire load condition was investigated by using the improved method. Simple two-dimensional analysis tools such as that adopted in this paper can be used to judge in a qualitative and quantitative the damage tolerance of buildings. The results of this example show that the proposed method can provide a better understanding of the failure mechanism of buildings due to different hazardous loading conditions. It can also be used to analyze the total response of structure to ground motions, impact, fire, and blasting hazardous.

REFERENCES

CSI, 2000. “SAP2000- intergraded Finite Element Analysis and Design of Structures.” Version 7.4, Computer and Structures, Inc., Berkeley, CA

Meguro, K., Iwashita, K., and Hakuno, M., 1991. Fracture analyses of structures by the modified distinct element method. *Structural Eng./Earthquake Eng.*, Vol.6, No. 2, pp. 283–294.

Meguro, K. and Tagel-Din, H., 1997. A New Efficient Technique for Fracture Analysis of Structures, *Bulletin of Earthquake Resistant Structure Research Centre, Institute of Industrial Science, the university of Tokyo*, No. 30.

Meguro, K. and Tagel-Din, H., 2000. Applied Element Method for Structural Analysis: Theory and Application for Linear Materials, *Structural Eng./Earthquake Eng.*, Vol. 17, No. 1, pp. 21-35

Meguro, K. and Tagel-Din, H., 2001. Applied Element Simulation of RC Structures under Cyclic Loading, *ASCE*, Vol. 127, No. 11, pp. 1295-1305,

Tagel-Din, H. and Meguro K., 2000[a]. Applied Element Method for Simulation of Nonlinear Materials: Theory and Application for RC Structures, *Structural Eng./Earthquake Eng.*, Vol. 17, No. 2, pp. 137-148.

Tagel-Din, H. and Meguro K., 2000[b]. Applied Element Method for Dynamic Large Deformation Analysis of Structures, *Structural Eng./Earthquake Eng.*, Vol. 17, No. 2, pp. 215-224.